1-1-1994

Dynamic phenomena in superconducting oxides by ESR

Juana Vivó Acrivos
San Jose State University, juana.acrivos@sjsu.edu

Lei Chen
San Jose State University

C. M. Burch
San Jose State University

P. Metcalf
Purdue University

J. M. Honig
Purdue University

See next page for additional authors

Recommended Citation

Juana Vivó Acrivos, Lei Chen, C. M. Burch, P. Metcalf, J. M. Honig, R. S. Liu, and K. K. Singh. "Dynamic phenomena in superconducting oxides by ESR" *Physical Review B* (1994): 13710-13723. doi:10.1103/PhysRevB.50.13710

Dynamic phenomena in superconducting oxides measured by ESR

J. V. Acrivos,* Lei Chen, and C. M. Burch
Department of Chemistry, San Jose State University, San Jose, California 95192-0101

P. Metcalf and J. M. Honig
Department of Chemistry, Purdue University, West Lafayette, Indiana 47907

R. S. Liu† and K. K. Singh‡
IRC in Superconductivity, Cambridge University, Cambridge CMB OH3, United Kingdom

(Received 13 May 1994)

Dynamic electron spin resonance (ESR) measurements compare the paramagnetic and antiferromagnetic (AF) properties of superconducting oxides in the range 4 K to room temperature, at 8 MHz and 9.36 GHz. Two are derivatives of $YBa_2Cu_3O_7$: I: $Nd(Nd_{0.05}Ba_{0.95})_2Cu_3O_7$, $T_{c0}=72$ K and II: $Y_{0.2}Ca_{0.8}Sr_2[Cu_2(Tl_{0.5}Pb_{0.5})]O_7$, $T_{c0}=108$ K and two are cases where AF ordering dominates the weak superconductivity: III: $NbO_{1.1}$, $1.25 \leq T_{c0} \leq 10$ K and IV: $La_2NiO_{4.00}$, $70\text{ K} \geq T_{c0} \geq 40$ K. At temperatures $298 \geq T \geq 64$ K, the ESR absorption by I indicates orthorhombic symmetry. The peaks at $g_c=2.06$, $g_b=2.13$, and $g_a=2.24$ are identified with the presence of 5% $Nd^{3+}(^4I_{9/2})$ in the Ba layer because the characteristic Cu^{2+} impurity hyperfine structure is absent and the ESR signal disappears several degrees below T_c. Near T_c the ESR absorption is reduced by two orders of magnitude. Proximity effects give rise to interference fringes with period $\tau_f(T)$ independent of the field **B** and the rate of sweep dB_z/dt. ESR is observed below T_c because flux penetrates the superconductor. The temperature dependence of τ_f leads to an activation energy for the flux motion $E_a(\text{I})/R \leq 16$ K and E_a (III)$/R \cong 3$ K $\simeq T_c/4$. In the superconducting state a coherent flux expulsion response to a change in B_z from 500 mT to zero is observed in times $\tau_r=8$ to 10 s. The inverse rate of noise spikes due to flux expulsion, when the samples are cooled through T_c in a magnetic field, varies from $\tau_{\text{noise}}=3.5$ s for III to 21 s for IV. The microwave absorption spectra identify three temperature regimes: (i) For $3.5\text{ K} < T < T_m \cong T^* < T_c$, superconducting behavior was confirmed by the energy loss near zero magnetic field and the kinetics of high-field noise due to flux expulsion. Near $g=2.00$ ESR absorption is observed for all materials. A broad absorption near 50 to 100 mT at 9.36 GHz has been attributed to AF resonance. (ii) $T_m \cong T^* \leq T \leq T_c$ identifies the range where flux motion gives rise to interference fringes in the ESR absorption. (iii) ESR and AF resonance are observed immediately after warming above T_c.

I. INTRODUCTION

Electron spin resonance (ESR) absorption near $g=2.00$ at $T < T_c$ has been reported for superconducting oxides.[1] The coexistence of paramagnetism and/or antiferromagnetism (AF) with superconductivity is important for the development of a theory of superconductivity in cuprates and other oxide superconductors.[2–4] To obtain further insight into the relationship between paramagnetism, AF, and superconductivity, the purpose of this work is to ascertain the dynamic interactions which can be deduced from the ESR absorption of four materials, (I) $Nd(Nd_{0.05}Ba_{0.95})_2Cu_3O_7$, $T_{c0}=72$ K, (II) $(Y_{0.2}Ca_{0.8})Sr_2[Cu_2(Tl_{0.5}Pb_{0.5})]O_7$, $T_{c0}=108$ K, (III) $NbO_{1.1}$, $1.25 \leq T_{c0} \leq 10$ K, and (IV) $La_2NiO_{4.00}$, $70 \geq T_{c0} \geq 40$ K, where these properties are well characterized in the literature.[3–8]

Charge neutrality in the unit cell may be achieved in $YBa_2Cu_3O_7$ by the presence of O^- and/or Cu^{3+} in layers O(3) and Cu(2).[5(i)] The Madelung potential $V=E_{\text{Madelung}}$ due to the charges Q on the ions depends on these charges and has been determined in $YBa_2Cu_3O_7$.[5(i)] The value of V for structures I–IV is evaluated in the Appendix. The strongest Madelung energy is obtained for IV (i.e., the most ionic), next is II, and the least ionic electrostatic interaction per formula weight determined by V is found for I and III. However V is just an approximation since the self-consistent-field (SCF) wave functions obtained for the conduction layer $(CuO_2)_n$ in the crystal field of the particular lattice[2(c)] show that the ionic charges in the conduction layers are reduced below the nominal value by shielding and covalency. The stability of these structures depends both on E_{Madelung} and the ground-state energy of the conduction states.

T_c for NbO has been reported in the recent literature to be near 10 K;[3(a)] this value may be due to defects and/or a solid solution of Nb in NbO,[3(d)] because a critical temperature $T_c=1.25$ K had been reported earlier for pure NbO.[3(d)] The properties of La_2NiO_4 and NbO depend on the sample doping and history in a magnetic field; superconductivity and AF ordering have been observed in these materials.[1(c),4] Takeda *et al.* have extensively investigated the properties of $La_{2-x}Sr_xNiO_4$ and there is considerable literature.[4]

ESR and energy-loss response near zero field[5,6] have been used in this work to compare the dynamic processes

in materials where superconductivity prevails (I and II) with those where AF ordering is dominant (III and IV) in order to ascertain some of the conditions which favor AF ordering and/or superconductivity.

II. EXPERIMENTAL

The samples were prepared as described in the literature.[4(b),5(c),7,8] Spectra are shown for crystallites and for selected $\simeq 0.1$ mg crystallites cast in 5 min epoxy (Devcon Corporation) and aligned in a magnetic field ($B_{al}=7$, 4, and 1.3 T) at room temperature. Spectra (Figs. 1 to 4 below) are shown as derivatives of the power absorption response dP/dB from an oscillating field $2iB_1\cos 2\pi\nu t$ ($\nu=8$ MHz and 9 GHz) vs B_z in a modulated external field $\mathbf{k}(B_z+2B_m\cos 2\pi\nu_m t)$ ($\nu_m=0.4$ to 10^5 kHz). These were obtained using a Varian 4250 and a Bruker 200 spectrometer equipped with an Oxford 900 cryogenic system.[9] When lock-in detection is used, the energy-loss signal is a modulated energy absorption in low fields by a superconductor. The acronym MEALFS is used to distinguish this response from standard ESR signals. Adrian and Cowan have reviewed the method recently.[5(h)] The response consists of two signals: O, the sharp discontinuity in the current (width less than 10 μT) when B_z passes exactly through zero due to the change in resistivity from exactly zero, and $(dP/dB)_0$, the energy loss observed in finite low fields several degrees below T_c. The fields B_1 and B_m (in a dual-cavity spectrometer [Ref. 9(b)]) were estimated using a free-radical reference, 1,1'-biphenylene 2-phenylallyl, with a very narrow ESR absorption of width $\Delta H_{ms}=50$ μT and $g=2.0027$.[9(a)] The broadening produced by $B_1, B_m > 50$ μT was used to estimate the field amplitudes: B_1 (μT) $\simeq 125\times 10^{-dB/20}$ (for an attenuation dB in decibels) and B_m (μT) $\simeq 2.32\times A_M$ (where A_M is the percent of the total modulation amplitude). The different parameters are specified for each spectrum. The temperature calibration for the Oxford ER900 was verified by placing a Au(Fe 3%)–Chromel thermocouple at the sample position. The accuracy was found to be better than the instability caused by the temperature control, as indicated in each spectrum. The exact zero field was ascertained first by the ESR absorption at 8 MHz of the free-radical reference and by the center of symmetry of the MEALFS signal determined after the first cooling cycle.[1(c)] In the dual-cavity spectrometer,[9(b)] the reference free radical is kept at room temperature, at a magnetic field higher than the sample, because a dc field is introduced at the latter to cancel the residual field of the iron magnet, in order to sweep through

$$B_z=0=B_{z,\text{laboratory}}+B_{z,\text{compensation}}\ .$$

The amplitude of the reference is used for quantitative analysis, i.e., the number of unknown spins $N(S)$ is determined for each spectrum given the relative amplitudes and the width of the unknown ESR absorption, ΔB_{ms} in mT.[9(b)] The ESR absorption of a known concentration of Mn^{2+} in HCl, in a 1-mm-i.d. capillary occupying the 1-in. sample space (where B_1 decreases from a maximum at the center to zero at the cavity edges with a sinusoidal dependence), was used to obtain the calibration

$$N_{\text{unknown}}(S)=\frac{f(T,A_M)}{S(S+1)}\frac{A_{\text{amplitude unknown}}}{A_{\text{amplitude reference}}}\times[\Delta B_{ms,\text{unknown}}(mT)]^2\ , \quad (1)$$

where $A_{\text{amplitude reference}}$ is determined to $\pm 10\%$ accuracy at scan rates $dB/dt\cong 2$ mT/s and

$$f(T,A_M)=A_M\times 5.3\times 10^{11}\times(T/298)$$

when Boltzmann statistics are obeyed and the line shapes are Lorentzian.

The samples were analyzed by x-ray diffraction and fluorescence using a Diano XRD8000 system.

III. RESULTS OF rf AND MICROWAVE MEASUREMENTS

The phenomena observed are categorized as follows. In the lowest-temperature regime (3.5 K to T_c) a nonresonance (MEALFS) response and high-magnetic-field noise (characteristic of flux expulsion by superconductors) are observed together with a broad AF resonance absorption derivative. Phase transitions are detected through changes in the ESR response.

Figure 1 shows the ESR data above and below $T_c=64$ K for I (apparent D^1_{4h} symmetry due to random -O-Cu-O- chains) and the parent compound $YBa_2Cu_3O_7$ (D^1_{2h} symmetry).[8(b),(d)] Figure 2 shows corresponding data for II (D^1_{4h} symmetry), where the Y layer has 80% Ca and the zeroth layer (containing -O-Cu-O- chains in $YBa_2Cu_3O_7$) has been replaced by planes of O centered about a square with Tl and Pb at the vertices.[8(a),(c)] Figures 3 and 4 show the same data for III and IV.

From $T=3.5$ K to T_c nonresonant energy losses (MEALFS signals) are present for all superconductors; high-field noise is observed in all the samples that were cooled through T_c in nonzero field. Cooling through T_c near $B_z=0$ eliminated the high-field noise for all samples. Though weak below T_c, a paramagnetic ESR absorption is observed near $g=2.00$ (Figs. 1 to 4). The data for the samples shown are reproducible after the sample has been cooled and warmed up to room temperature several times.

The ESR absorption derivative dP/dB_z near $g=2.00$ above an intermediate temperature $T_m\cong T^*$, 3.5 K $< T_m < T < T_c$, shows a superposition of interference fringes with a period $\tau_f(T)$ independent of the field sweep dB_z/dt at $\nu=9$ GHz [Figs. 1, 2(b), 3(b), and 3(c)]; the effect of the microwave field amplitude B_1 on the $NbO_{1.1}$ fringe period is shown in Fig. 3(c).

A broad anisotropic feature which remains unchanged up to T_c is observed at 9 GHz near 50–100 mT for all samples. Maximum intensity is observed in aligned $NbO_{1.1}$ [Fig. 3(b)] when the external field is parallel to the aligning field B_{al} and disappears when it is normal.

The time required for the field to relax from 500 mT to zero was determined in multiple-scan measurements by the echo of broad (10^2 mT) ESR absorptions at room

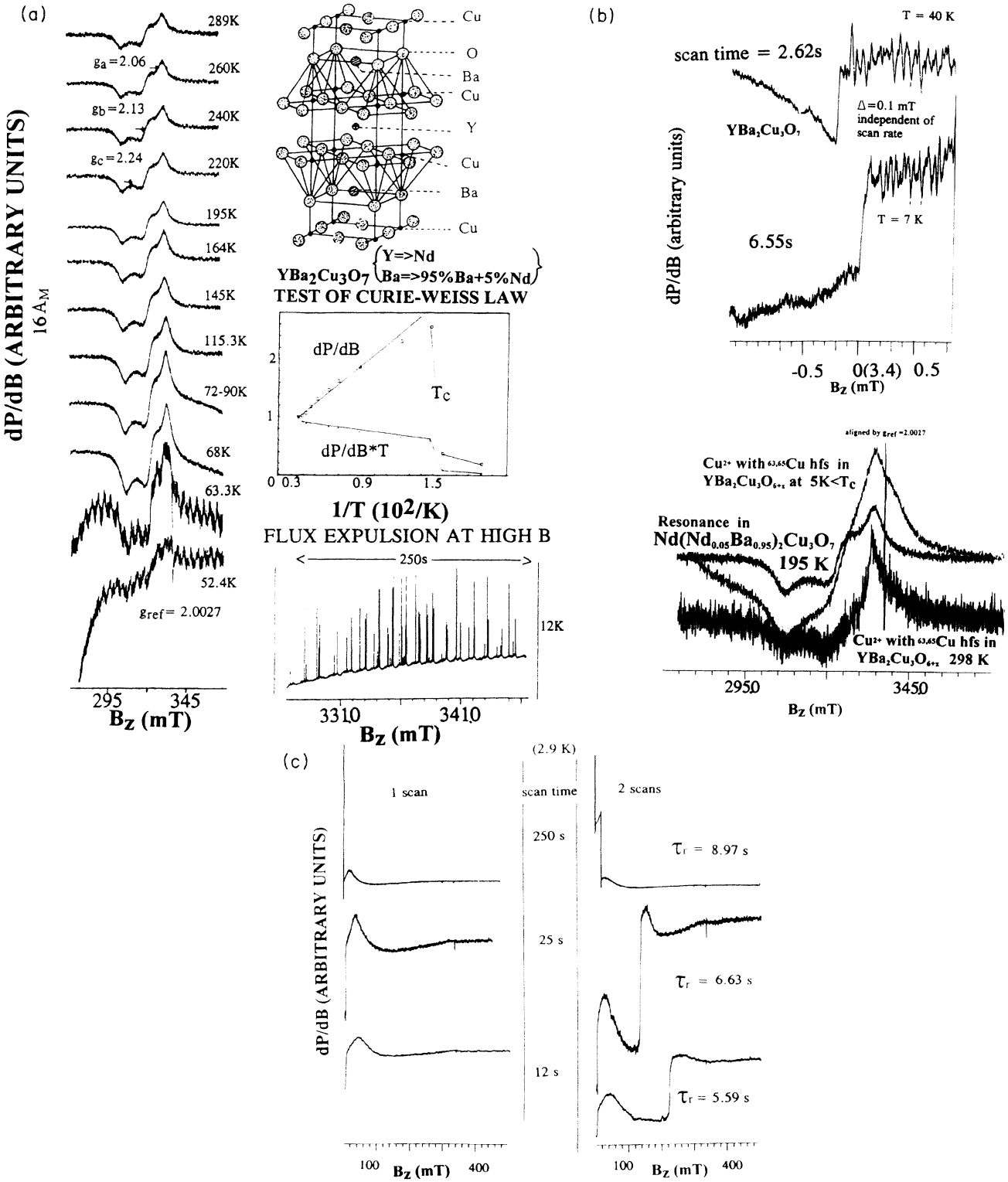

FIG. 1. I: $Nd_{1.1}Ba_{1.9}Cu_3O_7$. (a) Structure and ESR spectra vs T from room temperature to below T_c. Orthorhombic symmetry is indicated by the spectroscopic g values: $g_c=2.06$, $g_b=2.13$, $g_a=2.24$. Interference fringes are superposed on the ESR absorption below T_c; the period $\tau_f=11.5$ s is independent of sweep rate dB_z/dt. One insert shows how well the amplitudes of dP/dB and $T\,dP/B$ vs $1/T$ obey the Curie-Weiss law. The other insert shows the ESR spectra at 12 K, after cooling in a field in the region near $g=2$; noise expelled above H^* rides on top of interference fringes, at their crest. Autocorrelation of fringes and noise spikes is shown in Fig. 5 below. (b) Parent compound, $YBa_2Cu_3O_7$, showing MEALFS signal independent of temperature and dB_z/dt. The Cu^{2+} ESR absorption spectra obtained for $YBa_2Cu_3O_{6+x}$ at 298 K and 5 K are compared with the ESR absorption from I at 195 K. The asymmetry caused by the different relaxation times for the hyperfine components of $^{63,65}Cu^{2+}$ is definitely absent in the ESR spectra of I. (c) Flux expulsion (parent compound) in multiple-scan spectra. At very fast sweep rates τ_r depends on $B_z \geq 100$ mT.

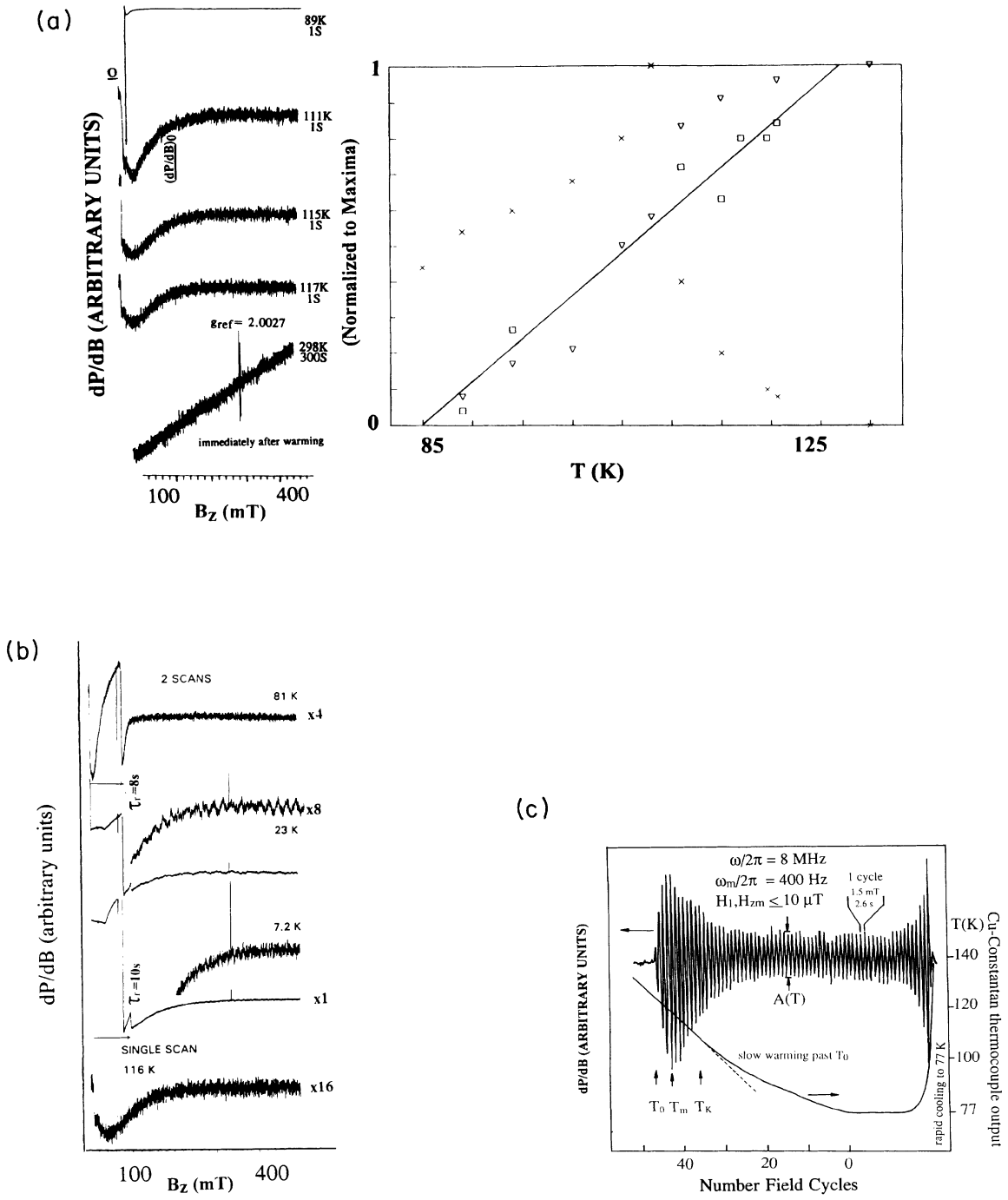

FIG. 2. II: $(Y_{0.2}Ca_{0.8})Sr_2Cu_2(Tl_{0.5}Pb_{0.5})O_7$. (a) Nonresonant (MEALFS) response ratio $r = O/(dP/dB)_0$. □, compared to the normalized (to maxima) heat capacity $\Delta C_{el}/\Delta C_{el,max}$ × and thermopower S/S_{max} ∇ obtained from Refs. 8(a) and 8(c). At 116 K the MEALFS signals up to 100 mT (AF?) are still observed, indicating that the method detects superconducting fluctuations above $T_c = 108$ K in the same manner as the nonvanishing ΔC_{el} and the thermopower [Ref. 8(a)]. The ratio r is nearly zero 20 K below T_c and approaches 1 only above T_c. The temperature where all superconducting fluctuations disappear is near 130 K. (b) Multiple-scan spectra showing two response times $\tau_r = 8$ and 10 s which suggest the presence of a minor phase leading to a broadening near 81 K. (c) Nonresonant (MEALFS) response measured at 8 mHz. The field is cycled through 0 every 2.6 s as the sample warms up. The temperature T is measured by a Cu-Constantan thermocouple wound around the sample immersed in the liquid N_2 bath, and the change in the slope dT/dt at $T_K = T_c$ (measured by heat capacity) indicates that the maximum in heat capacity was achieved at this temperature; T_M measures the maximum in $O + (dP/dB)_0$ and T_0 is the temperature where the sum disappears. These temperatures are comparable with the extrema in the thermopower data and the nonzero signals observed for ΔC_{el} in (a), i.e., the MEALFS signal, the heat capacity, and the thermopower measure properties above T_c that may be due to superconducting fluctuations and/or AF ordering.

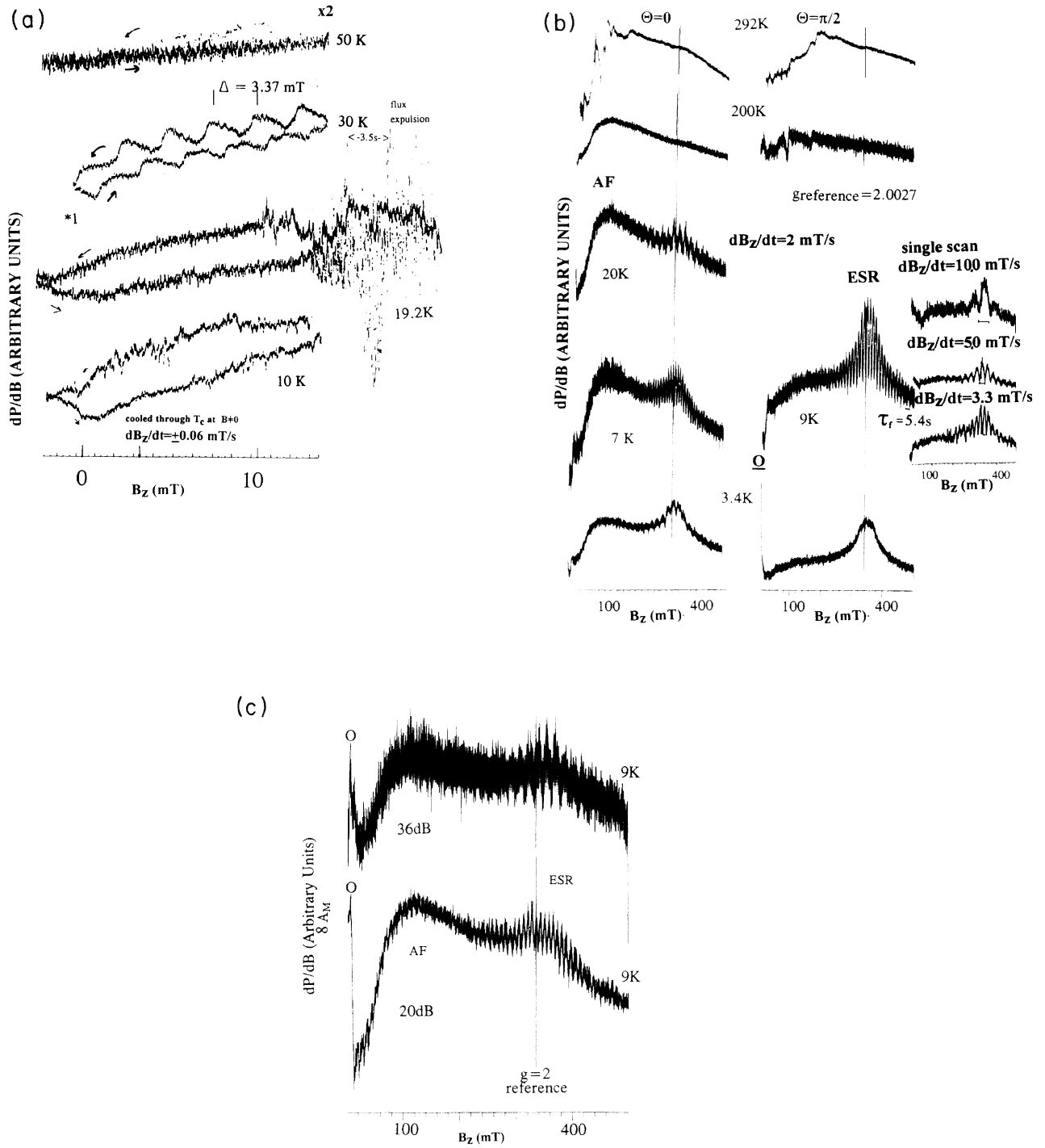

FIG. 3. III: $NbO_{1.1}$. (a) Nonresonant response (MEALFS) observed in the first cooling cycle for as-prepared material. The sample was exposed to 3.24 mT going through T_c down to 3.4 K. The spectra were recorded on warming. High-field noise is observed above 15 mT but this disappears completely when the dc field is static, even at 336 mT. The rate of flux expulsion of $\frac{3}{10}$ s is comparable to that observed for cuprates. The fine structure with separation Δ is explained by relation (3). The MEALFS signal disappears at 40 K and therefore must be due to a phase different from NbO. (b) Fraction of as-prepared material aligned at $B_{al}=7$ T ($\theta=\mathbf{B}_z \wedge \mathbf{B}_{al}$) cooled through T_c near zero field. AF resonance observed near 70 mT when $\theta=0$ (and disappearing for $\theta=\pi/2$) is independent of T and sharpens above 200 K but the intensity remains essentially constant, as expected for AF resonance. An isotropic ESR absorption near $g=2$ shows interference fringes. The inset (9 K, $\theta=\pi/2$) shows that the interference period τ_f is independent of the rate of field sweep dB_z/dt. (c) Saturation measurements at 9 K. The ESR absorption near $g=2$ saturates faster than that for the AF domains and the reference free radical and the period τ_f depends on B_1. (d) Room-temperature resonance for $\theta=0$. The spectrum between $g=28$ and 14 shows the hyperfine structure compared with the calculated spectrum for the Dysonian metallic ESR absorption, case A, with $A(^{93}\text{Nb})=1.04$ mT.

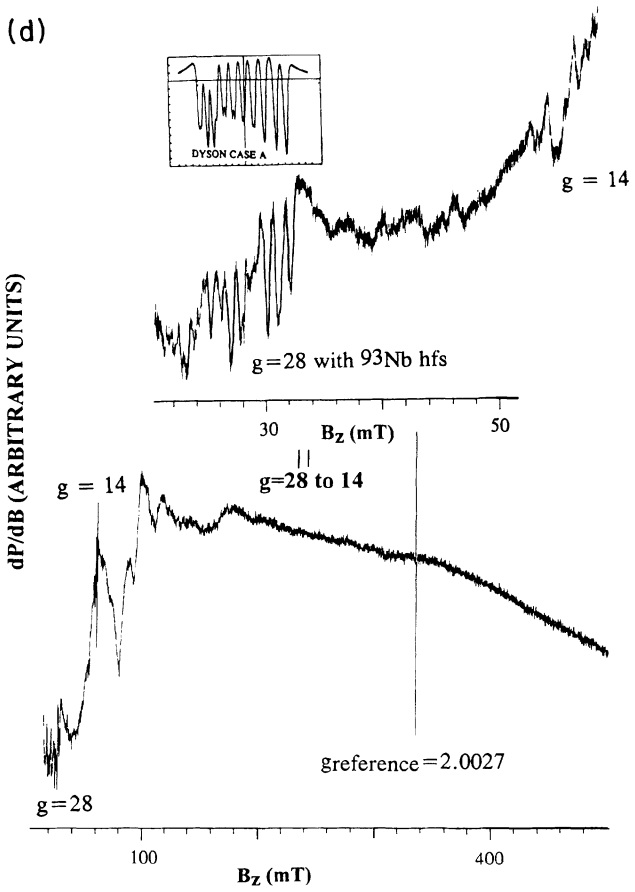

FIG. 3. (*Continued*).

temperature to be less than 4 s. However, in the superconducting state a coherent response to the change in magnetization is observed when the external field changes suddenly from 0.5 T to zero with a delay time τ_r of 8 to 10 s [Figs. 1(b) and 2(b)]. This response is absent for large signals (10^{-6} mole of reference free radical in the sample cavity).

IV. DISCUSSION OF RESULTS

X-ray diffraction and fluorescence and microprobe measurements confirmed the structures and the stoichiometry and the presence of single phases.[1(a),1(c),8(d)] The $h00$ and $hh0$ diffractions of III are in agreement with the pure NbO cubic structure reported by the National Bureau of Standards (U.S.) (150535). IV shows a fine structure for the 006 diffraction which is absent in nonsuperconducting La_2NiO_4.[1(c),4(e)] The main objective of the discussion is to identify the dynamic effects in the ESR absorption and to correlate the observations in the different temperature regimes in order to ascertain the properties of materials which are predominantly AF (III and IV) but also show properties attributed to classical superconducting behavior (I and II).

ESR absorption intensity [dP/dB in Fig. 1(a)] obeying the Curie-Weiss law is observed above T_c for I; it is associated with the presence of 5% Nd diluted in the Ba layer. The characteristic Cu^{2+} ESR absorption observed in oxygen-poor $YBa_2Cu_3O_{6+x}$ (with an anisotropic shape due to the relaxation time dependence on the nuclear spin quantum number for the $^{63,65}Cu$ hyperfine components) is compared in Fig. 1(b) with the ESR absorption of I. In $YBa_2Cu_3O_{6+x}$ the ESR of Cu^{2+} is observed below T_c and shows no proximity effects except for the Meissner effect field broadening observed when free radicals are in contact with a superconducting phase;[5(h)] it must be part of a different phase. Conversely higher concentrations of Nd^{3+} in the Ba layer, e.g., $I' \equiv Nd_{1.2}Ba_{1.8}Cu_3O_7$. $Nd_{1.3}Ba_{1.7}Cu_3O_7$ and $Nd_{1.4}Ba_{1.6}Cu_3O_7$ show very broad ESR absorption characteristic of spin-spin interactions,[10] with the concurrent lowering of T_c; the ESR absorption intensity of I' always decreases below T_c and disappears at all temperatures when the superconductivity is completely quenched by the Nd^{+3} concentration in the Ba layer.[8(e)] That is, the presence of Nd^{3+} in the Ba layer reduces the contact term at the Cu^{2+} end defects in the -O-Cu-O- chains in the 0th layer of I which are caused by its presence, but ESR absorption is always observed above T_c in the superconducting samples. Below T_c, the ESR intensity drops by over two orders of magnitude and for I shows interference fringes with a period $\tau_f = 11.5$ s near 52 K [Fig. 1(a)]; the ESR signal is very weak at 12 K $\cong T^*$, identified by the flux expulsion (Fig. 5); the noise spikes coincide with the crest of the interference fringes at $\tau_f = 14.3$ s, suggesting that the two may be connected, i.e., the motion of the flux lines may be associated with the flux expulsion; therefore the rates are comparable. The parent compound $YBa_2Cu_3O_7$ shows similar properties. Figure 6 shows two possible topologies for flux penetration into a superconductor,[6(c)] leading to ESR absorption. The Bohm-Aharonov proximity effect is said to be present because the ESR field does not penetrate the superconducting region; the interference is due to the different field alignment in the flux-penetrated regions; i.e., there is signal cancellation due to phase differences. When the flux lines move coherently between the different possible topologies these phases change so that the interference period measures the time of hopping between the topologies possible for flux penetration. Here a rate of $\frac{1}{10}$ s is reasonable when compared with the rate of flux hopping of $\frac{3}{10}$ s observed by electron microscopy in superconducting Nb.[6(d)]

The nonresonant response (MEALFS) is characterized for II. From $T = 4$ K to T_c [Fig. 2(a)], the two signals O and $(dP/dB)_0$ vary differently vs temperature; O is the only MEALFS response observed near 7 K, but as T increases a 50 mT broad response with peak amplitude $(dP/dB)_0$ appears near 89 K and the ratio $r \equiv (dP/dB)_0/O$ which vanishes at low temperatures and increases to unity as $T \to T_c$, can be used to compare the properties of I to IV. $O + (dP/dB)_0$ goes through a maximum at $T_M \geq T_c$ (determined by the heat capacity[8] C_p indicating that O and $(dB/dB)_0$ are not due to the same property. The ESR absorption near $g = 2$ is very weak but interference fringes are observed, indicating that some flux penetration occurs and that there is ESR absorption most probably in the Tl,Pb layer due to valence compensation in the structure II. Here the dynamics of

flux expulsion can be best measured when the field is turned off from 500 mT to zero. Figures 1(b) and 2(b) compare single-scan response with multiple-scan responses. When $B_z = 500$ mT is switched to zero, the recovery time is less than 4 s; a new scan is then started, with flux trapped at the high-field value; after a time $\tau_r = 8$ to 10 s flux is expelled in a single burst. This is independent of dB/dT and depends only on time and H. It is observed for all superconductors reported here. At 7.2 and 23 K, structure II exhibits two response bursts, suggesting that there are different phases and/or dynamic processes, though the x-ray diffraction indicates that the sample is a single phase; there is also weak ESR absorption showing interference fringes. At 81 K there is no ESR absorption and a single burst of flux expulsion is observed at $\tau_r = 8$ s, suggesting that τ_r depends weakly on temperature; Fig. 1(b) shows that τ_r at different scan rates depends on B_z, but that the broad feature (50–100 mT) remains unchanged.

The nonresonant MEALFS response near zero-field $B_x = 0$ [O when B_z passes exactly through zero and $(dP/dB)_0$] must arise from phenomena that occur close to T_c. A possible cause[5] is that energy loss occurs when the flux varies discontinuously across Josephson junctions found in granular samples; according to Kittel,[6(a)] the expression for $i(\mathbf{B})$ is then

$$i(\mathbf{B}) = i_{\max} |\sin(\pi \mathbf{B} \cdot \mathbf{A}_{J,t}/\Phi_0)/(\pi \mathbf{B} \cdot \mathbf{A}_{J,t}/\Phi_0)| , \quad (2)$$

where $\Phi_0 = h/2e = 2.067 \times 10^{-15}$ Wb is the quantum unit of flux, and $A_{J,t}$ is the magnitude of the total area of the Josephson junction, with the unit vector along the normal direction (equivalent of the Fraunhofer relation). The periodicity of $i(\mathbf{B})$ gives rise to a fine-structure signal near zero field in single crystals.[5] For randomly oriented powders, averaging is done,[5(c)] over orientations $\mathbf{A}_{J,t} \wedge \mathbf{B} = 0$ to $\pi/2$; the width between the points of max-

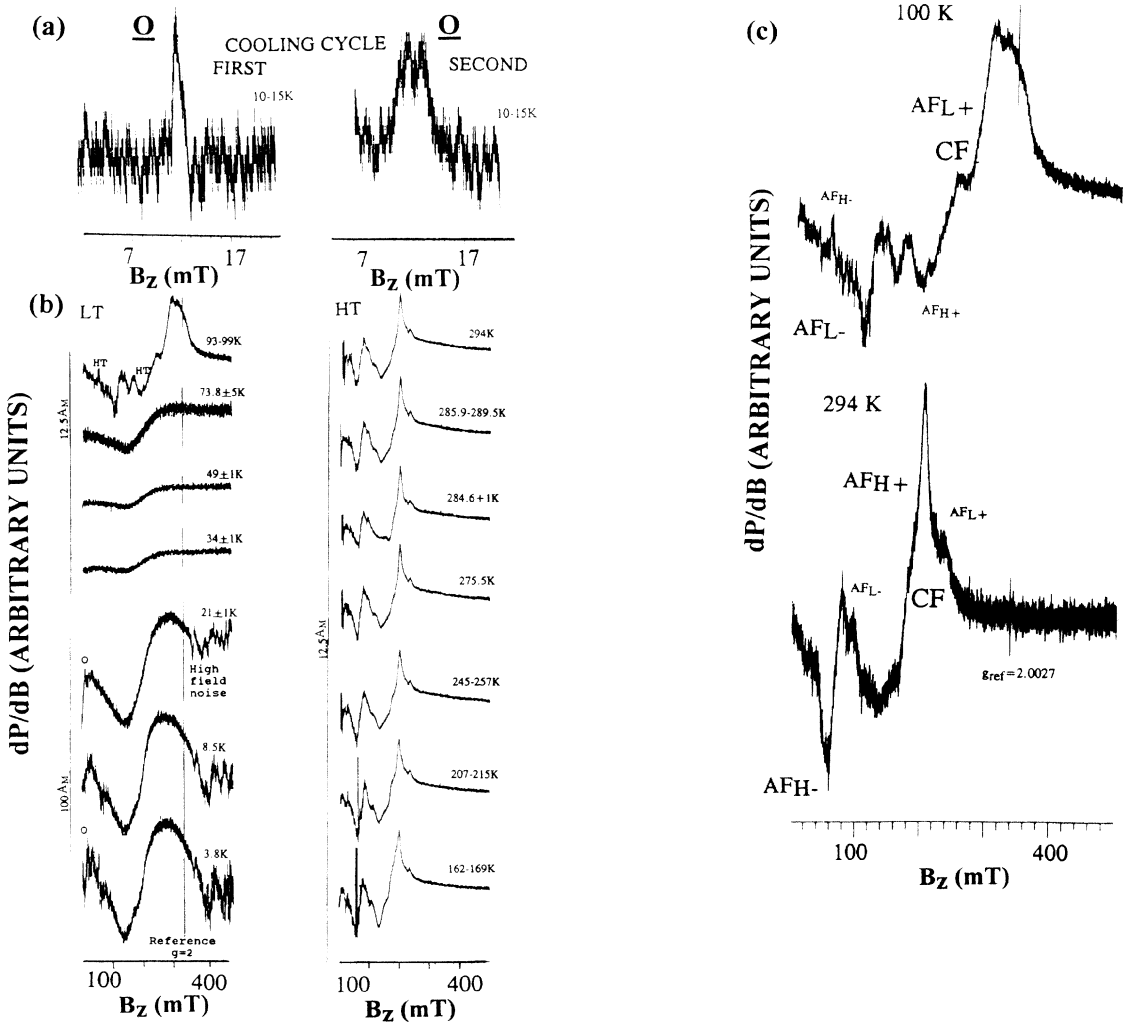

FIG. 4. IV: $La_2NiO_{4.00}$. (a) Nonresonant response O near 10 to 15 K. (b) Nonresonant response and AF resonance vs temperature. The high-field noise gives a rate of flux expulsion of $\frac{1}{21}$ s which is not as fast as for the other three materials. (c) AF resonance below and above the phase transition near 160 K. The center-field (CF) resonance identifies the nonaligned domains and is centered about the extrema $AF_{\pm}$. The subscripts H and L identify the high- and low-temperature phases and, the presence of the minority phases above and below 160 K indicates that hysteresis is present.

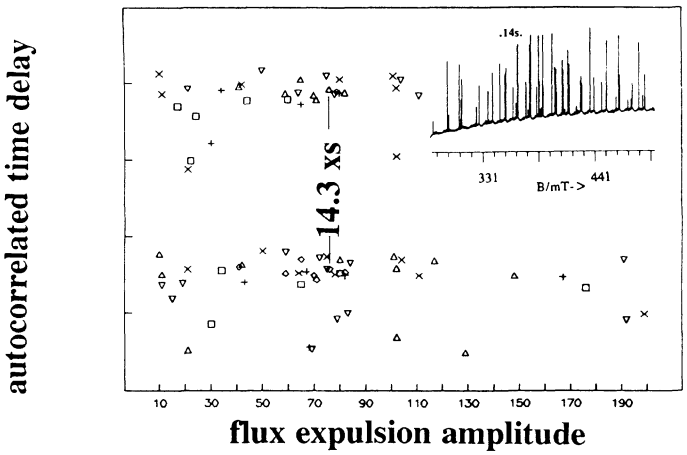

FIG. 5. Autocorrelation of the noise spikes observed in the ESR absorption form I in Fig. 1(a) near 12 K. On the abscissa is recorded the amplitudes of the noise spikes, and on the ordinate the time axis displaced by $14.3x$ s (x = integer) for all the noise spikes. The displacement x was varied to obtain a best fit for the rate process of one per 14.3 ± 0.5 s.

imum slope, $\Delta B_{z,ms}$, is

$$\langle \Delta B_{z,ms} A_{j,t} \rangle = 0.5 \Delta B_{z,ms} \langle A_{j,t} \rangle = 1.3\Phi_0 \ . \quad (2')$$

The linear dimension of the Josephson junction for powders and single crystals follows from (2'):

$$\langle A_{j,t} \rangle^{1/2} = (2.6\Phi_0/\Delta B_{z,ms})^{1/2} \ , \quad (3)$$

$$\langle A_{J,t} \rangle^{1/2} = (\Phi_0/\Delta B_{z,\text{crystal}})^{1/2} \ . \quad (3')$$

The superconducting behavior of $NbO_{1.1}$ and $La_2NiO_{4.00}$ is identified by the nonresonant response (MEALFS) signals and the high-field noise due to flux expulsion when the samples were not cooled in zero field. Figure 3(a) shows the data for structure III in the first cooling cycle; from 3.4 to 10 K typical superconducting hysteresis in $(dP/dB)_0$ is observed; noise is observed for $NbO_{1.1}$ above 15 mT and near $g=2$ at intervals of $\simeq 3.5$ s; however, the noise disappears in both low and high fields when the field is static. Between 23 and 37 K a fine structure that can be explained by relation (2) is observed, and must be due to a minority phase different from pure NbO. Table I reports the linear dimensions of $A_{J,t}$ deduced using relations (3) and (3'). Fine structure is observed for all samples near T_c, except for IV.

Interference fringes superposed on a Dysonian-shaped ESR absorption near $g=2$ are also observed for $NbO_{1.1}$ cooled through T_c in zero field, ascertained in the first cooling cycle [Figs. 3(b) and 3(c)]. The period τ_f (Table II) is independent of the sweep rate dB_z/dt and $\theta = \mathbf{B}_z \wedge \mathbf{B}_{al}$ but depends on temperature and microwave power [Figs. 3(b) and 3(c)].

Relation (1) gives $N(\text{III}) \simeq 1$ μmol ($S=\frac{1}{2}$) per mol of NbO for the $g=2$ microwave absorption intensity; this is reasonable taking into consideration that the flux-penetrated regions in I were found to be less than 1% near T_c. This signal saturates easily near 9 K [Fig. 3(c)] and obeys the Curie-Weiss law from 11 to 40 K. In addition to the ESR absorption near $g=2$, the broad features centered near 70 mT are associated with AF ordering. The latter are broad when nonresonant signals are observed and sharpen above T_c for III and IV [Figs. 3(b) and 4(a)].

$La_2NiO_{4.00}$ (Fig. 4) exhibits properties that are very similar to III. The AF resonance is broad when the nonresonant (MEALFS) signal is present and sharpens between 70 and 90 K when it disappears; a phase transition is observed near 160 K, and above this temperature the spectra remain unchanged to 294 K.[1(c)]

The sample changes that occur immediately after repeated cooling cycles are made evident in II [Fig. 2(a)]; a

TABLE I. Linear dimensions of Josephson junction deduced from $(dP/dB)_0$ using relations (3) and (3'). The maximum values of the values of the ratio $r(T_c)$ are also given.

Superconductor (T range)	$\Delta B_{z,\text{fine}}$ (oriented) (mT)	$\Delta B_{z,ms}$ (width) (mT)	$\langle AJ,t \rangle^{1/2}$ (μm)	$r(T_c)$
$Nd_{1.1}Ba_{1.9}Cu_3O_7$ (12 K)	0.6		2	<1
$(Y_{0.2}Ca_{0.8})Sr_2[Cu_2Tl_{0.5}Pb_{0.5}]O_7$ (77–130 K)	0.7		1	<1
$NbO_{1.1}$ (23–40 K)	3.37		0.5	1
$La_2NiO_{4.00}$ (15–40 K)		0.5	2	>1

TOPOLOGY OF FLUX AND SPIN ALIGNMENT IN SUPERCONDUCTORS

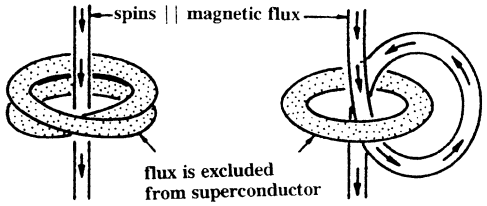

FIG. 6. Two possible topologies for the penetration of flux in a superconductor according to Ref. 6(c). The interference fringes and the noise spikes may be caused by coherent flux jumps changing the spin alignment in the coiled configuration, especially if the excitation modes from the CuO chain layer to the CuO_2 layer, influencing the magnetic properties in the non-superconducting Ba layer.

broad ESR absorption is observed, immediately after the cooling cycle, from T_c up to room temperature, suggesting that the signal is due to AF resonance. This disappears with time and no ESR absorption is observed after some days.

Chemical dynamics are deduced from the ESR spectra.[10] The ESR interference fringes below T_c are said to be caused by Aharonov-Bohm proximity effects,[6(b)] because changes in the superconducting region, which is not accessible to ESR measurement, are responsible. The interference effects are produced by the modulation of phase differences $\Delta\phi=0$ to π (due to different spin alignments in the flux-penetrated regions) by the coherent flux jumps between the topologies shown in Fig. 6. These are not observed at 3.5 K; they appear at an intermediate temperature $T_m \cong T^* \leq T_c$ [Fig. 3(b)], suggesting that the flux motion is activated. Peshkin and Tonomura[6(c)] have shown that the phases of the electron beams passing within and outside superconducting Nb toroids differ by $\Delta\phi=0$ or π. A qualitative explanation is provided in terms of the topologies shown in Fig. 6 if the flux lines move from one topology (straight) to another (twisted) in times of the order of τ_f. It has been shown that the current oscillations in the vortex lattice occur at microwave frequencies.[6(j),6(k)] When these are comparable to $\nu=9.36$ GHz of the ESR measurement a transformation to the rotating frame[11] shows the motion of the flux lattice which appears as an interference between the signals produced by the penetrating fields in a manner not unlike the light interference detected when a moving sector is placed in front of the light source. The chemical dynamics of flux motion detected by ESR is then written

$$e_2^{2-}(\uparrow\downarrow \mathrm{SC})\ (\text{flux jump}) \rightarrow e^-(\uparrow \mathrm{ESR}) + e^-(\downarrow \mathrm{ESR}) , \quad (4)$$

where the $e_2^{2-}(\uparrow\downarrow \mathrm{SC})$ represent the superconducting pairs where the arrows indicate the direction of the spins; these dissociate into the free spins detected by ESR $e^-(\uparrow \mathrm{ESR}) + e^-(\downarrow \mathrm{ESR})$ at the rate of flux jumps. The spin transition is forbidden and is as slow as phosphorescence. At the instant of dissociation the ESR spins in (4) are of opposite phase; their absorption signals should interfere destructively but the twisting of the flux tubes in Fig. 6 will change their relative alignment leading to constructive interference. In order to observe the macroscopic, reproducible interference signal shown in Fig. 1(a) the so-called "*chaotic motion of flux above* T^*" must be coherent and follow an attractor path. This is in agreement with the elegant Lorentz microscopy of Tonomura,[6(d)] showing the real time motion of flux in Nb and high T_c cuprate films above T^*. The first-order rate constant is

$$1/\tau_f = k(\text{flux motion}) = k_{f0}\exp(-E_a/RT) , \quad (4')$$

where $E_a(\mathrm{I})/R \cong 16\ \mathrm{K} \simeq T_c/4$ (52–12 K) and E_a/R (III) $\simeq 3$ K (4–9 K).

TABLE II. Features of the $NbO_{1.1}$ spectra: Relative amplitudes for the ESR absorption ($g=2$) and AF resonance (near 100 mT), and interference period τ_f for absorption centered near $g=2$.

$T\pm2$ K	$\frac{TA_{(g=2)}}{A_{\text{reference}}}$[a] (±10%)	$\frac{A_{\text{fringes}}}{A_{(g=2)}}$ (±10%)	τ_f (s)	$\frac{A_{(\mathrm{AF},\theta=0)}}{A_{\text{reference}}}$[b] (±10%)	B_1[c] (μT)	$B_m(10^5$ Hz) (μT)	dB_z/dt (mT/s)
3.4	1	0	9.2	0.8	7.9	20	2
9			4.8		14	20	2
9	4	1	5.4	0.8	7.9	20	2–10
9			7		4.4	20	2
9			7.9		2	20	2
20	3	1	9.6	0.8	7.9	20	2
40	4	1		0.8	7.9	20	2
48				0.8	7.9	20	2
70				0.8	7.9	20	2
100				0.8	7.9	20	2
292				1			

[a]The Curie-Weiss law appears to be satisfied from 11 to 40 K. This would apply if the flux penetration was constant in this temperature interval, $T > T^*$. Near 4 K the ESR is saturated [Fig. 3(c)].

[b]The AF resonance sharpens above 200 K.

[c]The absolute uncertainty in B_1 and B_m is large but the relative values of B_1 are accurate to within the figures given.

Little,[12(a)] Ando *et al.*,[12(b)] and Yu, Lee, and Stroud[12(c)] have also observed interference effects in measurements of the conductivity of normal metals in the proximity of superconducting regions. The period τ_f (Table II) is independent of the field modulation frequency (100 and 50 kHz), but decreases as the microwave field amplitude B_1 is increased and the ESR absorption is saturated, suggesting that the rate process is complicated by the presence of B_1.

The coherent response to a rapid change in magnetization when B_z goes from 500 mT to zero below T_c (Figs. 1 to 3) is independent of $dB_z/dt = 2$ to 10 mT/s and starting field; the response signal must arise from rate processes which change the relative size of normal and superconducting regions as a function of the external field. Since the time required for the field to relax to zero was determined to be less than 4 s, the sample experiences the applied field in 4 s; however, it appears that it takes longer to expel the flux trapped at high fields. Harada *et al.*[6(d)] have shown that after switching a field of 0.15 mT to zero in 5 s there remained 10% trapped vortices; these moved slowly towards a void in the film where they eventually disappeared. The coherent flux expulsion in Figs. 1(b) and 2(b) indicates that the flux which penetrated at 500 mT is not expelled immediately after the external field is reduced to zero (it supersaturates), and as the field increases it is eventually expelled, taking a time τ_r to reach equilibrium (expelling the excess in a burst); there is a field effect [Fig. 1(c)] which suggests that τ_r can be shortened by increasing B_z. Thus, τ_r measures the time required to reach equilibrium when flux is added to a critically supersaturated system which must also depend on the motion of flux.[6(f)]

The three rate processes measured by $1/\tau_f$, $1/\tau_r$, and $1/\tau_{\text{noise}}$ are all of the same magnitude (several seconds). The motion of flux can damage the sample, especially when it is all expelled in a single burst. It is therefore not surprising that the room-temperature ESR absorption in the best superconductor II shows hysteresis [Fig. 2(a)]. In some cases the defects can be annealed at room temperature (e.g., II) but in others the damage is annealed only at high temperatures (e.g., IV).[4]

AF resonance (the broad feature near 50–100 mT) sharpens above T_c but remains unchanged up to room temperature. The AF resonance condition is given by Kittel for $B_z = 0$:[6(a)]

$$(h\nu/g\beta)^2 = B_A(B_A + 2B_E) , \tag{5}$$

where B_E is the exchange field and B_A is the axial field. Assuming partial alignment in an external field B_z, the anisotropy field in uniaxial antiferromagnets goes from $B_A \| B_z > 0$ to $B_A \pm B_z$ [in relations (46) and (47), Chap. 16, of Ref. 6(a)]. The resonance condition in Figs. 3 and 4 is then

$$(h\nu/g\beta - B_z)^2 = B_A(B_A + 2B_E) , \tag{5'}$$

or

$$B_{\text{AF}_\pm} = B_z \simeq |2B_AB_E|^{1/2}|1 + B_A/4B_E| \pm |h\nu/g\beta| . \tag{6}$$

This sets the AF resonance field at $\pm(2B_AB_E)^{1/2}$ around $h\nu/g\beta$. For strong AF alignment, e.g.,

$$B_E(\text{MnF}_2) = 54 \text{ T} \gg B_A(\text{MnF}_2) = 880 \text{ mT}$$

at 0 K,[6(a)] a spectrometer operating at 9 GHz may not necessarily detect the AF resonance.[6(g)] However, for structures III and IV, $|B_AB_E|^{1/2}$ is of the order of several mT. The resonance fields $B_{\text{AF}_\pm}$ in (6) are achieved for $La_2NiO_{4.00}$ [Fig. 4(c)], giving $|B_AB_E|^{1/2} = 131.6$ and 197.2 mT and $g = 10.6$ and 8.1 from 294 to 162 K and 162 to 90 K, respectively. The phase transition near 160 K reduces $|B_AB_E|^{1/2}$, suggesting that either there is motional narrowing of the spin-spin interactions[10] above 160 K, and/or that there is canting of the interacting spins. There is evidence for the presence of the unstable phase above and below the phase transition in the ESR spectra in Fig. 4(c), suggesting that there is hysteresis. The Néel temperature is above 298 K for NbO and La_2NiO_4.[3(e),4] The AF resonance linewidths (Figs. 3 and 4) indicate that there is an exchange reaction between AF states and other states below T_c, with a rate constant determined from the linewidth, $k = 1/T_2 \simeq 10^{10}$/s; the other states may be the source of the nonresonant energy loss (MEALFS signal).

High-temperature ESR absorption is observed for all materials immediately after cooling. $NbO_{1.1}$ and $La_2NiO_{4.00}$ exhibit sharp resonances in very low fields. These type of resonances have been observed in semiconductors.[1(c),6(e),6(f)] For $La_2NiO_{4.00}$ (Fig. 4) these are observed in a narrow temperature regime (160–215 K). For $NbO_{1.1}$ [Fig. 3(d)] these appear above 200 K; near room temperature there is a very little ESR absorption near $g = 2$ and the low-field resonance is orientation dependent, repeating every 180°. NbO is a cubic crystal with the rocksalt structure, missing 25% of the anion and cation sites.[3(b)] Since the ESR spectra repeat only after a 180° rotation about the external field, the magnetic site must have less than cubic symmetry, which suggests the absorber is associated with the excess oxygen. The ^{93}Nb hyperfine structure observed in the ESR absorptions at low fields, especially for the nearly orientation-independent absorption centered near $g = 28.6$, can help in the assignment of an impurity magnetic site in $NbO_{1.1}$. The total number of spins is estimated using relation (1) as $N(\text{III}, S = \frac{3}{2}) \simeq 2$ mmol per mol NbO. The low-field isotropic ESR absorption is most probably a $\Delta S_z = \pm 2, \Delta I_z = 0$ transition associated with the more intense orientation-dependent $\Delta S_z = \pm 1, \Delta I_z = 0$ transition centered near $g = 14.3$. The Hamiltonian describing this impurity state must obey the relations (9.80)–(9.82) of Ref. 10, including the crystal-field effects. The complete assignments require single-crystal measurements. However, it is important to note that the dipolar terms D and E in the above Hamiltonian must be negligible relative to the ^{93}Nb hyperfine coupling constant A, giving rise to nearly orientation-independent sharp transitions at room temperature. The broadening of these transitions at low temperatures above T_c indicates that there is coupling to other magnetic states which cannot contribute to the linewidths at room temperature, most probably because of very short relaxation times which cannot couple to the

ESR characteristic times.[10] As the temperature decreases, the relaxation times increase to values comparable to the ESR characteristic times and may give rise to the broadening through the spin-spin coupling.[10,11] The $\Delta S_z = \pm 2, \Delta I_z = 0$ transitions are forbidden in the ESR spectrometer configuration (i.e., $\mathbf{B}_1 \perp \mathbf{B}_z$) and are weaker than the $\Delta S_z = \pm 1, \Delta I_z = 0$ transitions, but in this material nonlinear effects can give rise to a component $\mathbf{B}_1 \| \mathbf{B}_z$. Two O^- ions can create an axial crystal field near an isolated $Nb^{2+}(^4F)$ which gives rise to the observed hyperfine structure; second-order hyperfine interactions alone do not reproduce the observed data for a metallic Dyson case-A ESR absorption when the dipolar contribution is of the order of $|A|/4$ where $A(^{93}\text{Nb}) = 1.04$ mT [Fig. 3(d)], suggesting that there are weak contributions from the D and E terms in the Hamiltonian.

V. CONCLUSIONS

There is evidence for paramagnetism and antiferromagnetism in the ESR spectra of structures I to IV. I represents a case where the dynamics of flux motion can be measured by ESR spectroscopy in a superconductor. The exact ESR absorber sites cannot be identified at this time, but the phenomena observed in the superconducting state have been associated with the flux motion in the superconductor: The interference fringes superposed on the $g = 2$ ESR absorption are caused by Aharonov-Bohm proximity effects; the response to the change in magnetization indicates that there is more than one phase and/or dynamic process to expel flux trapped at $H = 0.5\ \text{T} > H^*$ and is a simple method to verify phase purity. The flux expulsion indicates that cycling to high magnetic fields can produce permanent damage to a superconducting sample. From T_c to room temperature the AF resonance remains essentially unchanged for $NbO_{1.1}$ and $La_2NiO_{4.00}$, i.e., $T_{\text{Néel}} > 300$ K.[3(e),4(a)] The ESR absorbers are in a crystal field of lower symmetry than the bulk for both $NbO_{1.1}$ and $Nd_{1.1}Ba_{1.9}Cu_3O_7$; the room-temperature ^{93}Nb hyperfine structure indicates the ESR absorber is not in a cubic site in $NbO_{1.1}$, while the g factors indicate that the symmetry in the vicinity of the absorber is orthorhombic in $Nd_{1.1}Ba_{1.9}Cu_3O_7$. The sharpening of the AF resonance signal above T_c suggests that the superconducting and AF domains are in close proximity, and that the former provide a relaxation channel for the latter. Even though the composition of the sites giving rise to the paramagnetic, AF, and superconducting signals in the host lattices cannot be ascertained by ESR, the proximity effects suggest that the different domains were formed at the same time and that they depend on the sample history (cooling and exposure to magnetic fields). The predominance of nonresonant energy absorption (MEALFS signal) for I and II and of AF resonance for III and IV indicates that the change in the Gibbs free energy near T_c for the first two favors superconductivity over AF alignment and that the opposite is true for the latter two. The fact that the activation energies for reaction (4) are of the order of $T_c/4$ suggests that the flux motion is coherent and determined by the energy gap. The theory by Alexandrov and Mott[2(d)] gives a value for the interplane hopping integral $t_\perp \cong T_c/4$ which suggests that E_a is dominated by flux motion between planes; this is of some importance in the case of I because it suggests that superconductivity occurs both in the CuO chains layer, as suggested recently,[5(l)] and in the CuO_2 layer.

ACKNOWLEDGMENTS

This work was carried out at SJSU with support from NSF Grants No. DMR 8921163, No. DMR 9307387 and No. INT 8922483; at Purdue University with support from DOE Grant No. De-FG02-90ER45427 MISCON. J.V.A. is most grateful to Professor Y. Liang of the IRC for his hospitality and to Professor N. F. Mott for discussions on the theory of superconductivity while spending a sabbatical leave at the IRC in Superconductivity, Cavendish Laboratory, and for suggesting that NbO was a material where the coexistence of superconductivity and AF alignment would be possible. Professor M. P. Klein and Professor C. Jeffries are also thanked for their shared insight.

APPENDIX: MADELUNG ENERGY CALCULATIONS FOR THE STRUCTURES I–IV

The potential energy in an ionic crystal yields the Madelung energy V.[13] Ewald[14] and Born and Kun[15] developed the Ewald method used for these structures.[5(i)] Rapid convergence is obtained here by summing V making use of the crystal symmetry and the order of the crystal growth, i.e., by layers in the structures I to IV [Fig. 7(a)]:

$$E_{\text{Madelung}} \equiv V = \sum Q_{i000} Q_{jHKL} / R_{i000,jHKL} = V_{000} + \sum_{HKL} V_{HKL} \ . \tag{A1}$$

Here Q_{i000} is a charge at site i of the origin unit cell separated by $R_{i000,jHKL}$ from Q_{jHKL} at site j of all the cells in the crystal, obtained by translating the origin from (0,0,0) to (aH, bK, cL) along the principal axes (a,b,c) in Fig. 7(b).

$$V_{000} = \sum_{i,j}{}' Q_i Q_j / r_{ij}$$

is the contribution to the electrostatic energy from one unit cell, and the crystal symmetry determines the rest of V, i.e.,

$$V_{HKL} = \sum_{i,j} Q_i Q_j / R_{HKL} \sum_l P^l(\cos\theta_{ij})(r_{ij}/R_{HKL})^l$$

is due to the interaction of the origin unit cell with the rest in the Legendre polynomial expansion of V. Contributions to V_{HKL} from the terms $l = 0, 1$ vanish by virtue of charge neutrality and symmetry; $R_{HKL}^2 = a^2H^2 + b^2K^2 + c^2L^2$ and the addition theorem of spherical harmonics[10] give in Fig. 7(b)

$$V_{HKL} = \sum_{ij} Q_i Q_j r_{ij}^2 / R_{HKL}^3 \sum_{l \geq 2} P^l(\cos\theta_{ij})(r_{ij}/R_{HKL})^{l-2} \ ,$$

indicating that summing (A1) one layer at a time leads to a rapid convergence because the leading terms in V_{HKL},

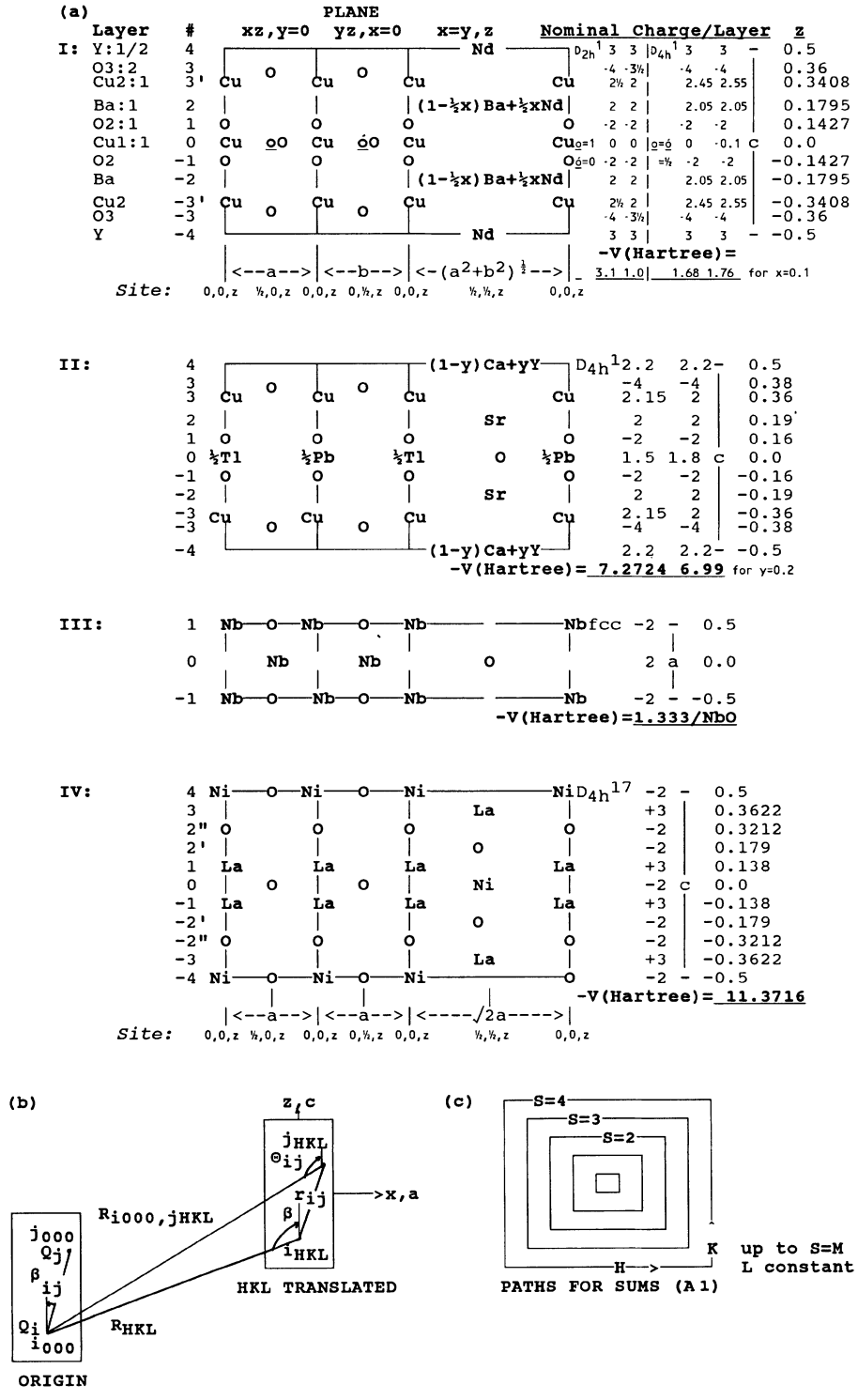

FIG. 7. Parameters for the electrostatic interaction in an ionic crystal. (a) Clinographic projections of structures I to IV along the $x,z(y=0)$, $y,z(x=0)$, and $x=y,z$ directions, indicating the composition and plausible average layer charge determined by the valence fraction f_v where $v=-1$ and -2 for O, 1, 2, and 3 for Cu, 2 and 4 for Pb, and 1 and 3 for Tl atoms, and o and $\acute{o}$ are the occupation numbers for the O(1) sizes in the zeroth layer of $YBa_2Cu_3O_7$, subject to charge neutrality. The respective values of V obtained by (A3), using literature unit axes (Refs. 3, 4, 8) are shown for two extreme values of layer charges. (b) Charges Q_i at sites i in the unit cell; $(R_{HKL}\beta,\alpha)$ are the spherical polar coordinates of the vector connecting two identical sites between the translated cells; $(R_{i000,jHKL},\theta_{ij},\phi_{ij})$ are the spherical polar coordinates of the vector connecting two different sites in the translated cells, and $(r_{ij},\beta_{ij},\alpha_{ij})$ are the spherical polar coordinates of the vector connecting sites within the same unit cell. (c) Summation paths by shells S for (A1) in a given layer.

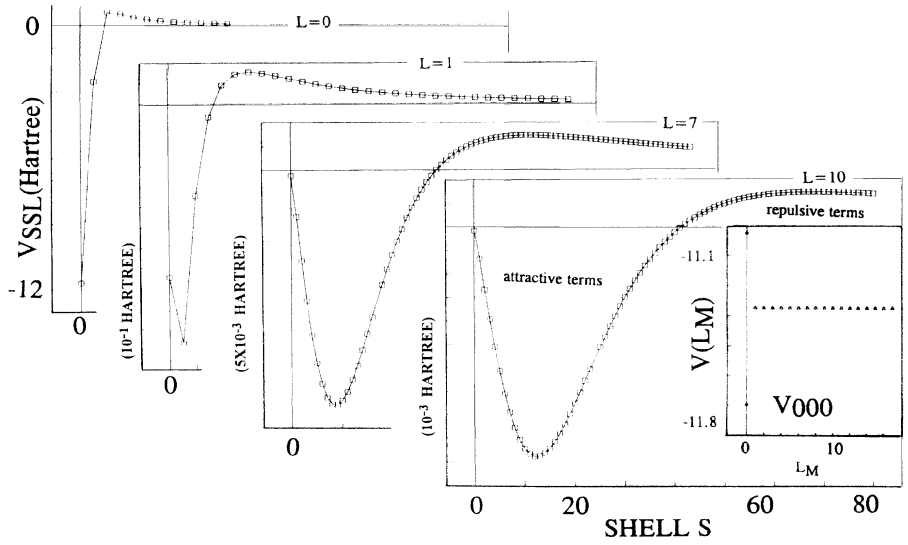

FIG. 8. $V_{SSL}(La_2NiO_{4.00})$ contributions versus shell S shown in Fig. 7(c), for different values of L. The inset shows how $V(L_M)$ approaches convergence with increasing L.

$$V^{(2)}_{HKL}=\sum_{ij} Q_i Q_j r_{ij}^2/R^3_{HKL}P^2(\cos\beta)P^2(\cos\beta_{ij})\ , \qquad \text{(A2)}$$

have attractive and repulsive contributions that nearly cancel out (Fig. 8). (A1) is summed up to shell $S=M$ [Fig. 7(c)] estimating the terms left out by integration, using the symmetry of $V^{(2)}$, i.e.,

$$V(L_M)=\sum_{L=-L_M}^{-L_M}\sum_{H,K} V_{HKL}$$

and (A3)

$$V=V(L_M)+V_{\text{correction}}\ ,$$

where the path is $H=S$, $K=-S$ to S and $K=S$, $H=1-S$ to $S-1$ up to $S=M$.

$V_{SSL}=\sum_{\text{shell } S} V_{HKL}$ versus S for different values of L in $La_2NiO_{4.00}$ is shown in Fig. 8. The symmetry is such that attractive shell terms are nearly canceled by the repulsive ones, giving a negligible total contribution per layer for $L\geq 1$. V_{SSL} approaches $V^{(2)}$ symmetry as S increases, which is verified by the fact that V_{SSL} vanishes when

$$\cos\beta=cL/(c^2L^2+a^2S^2+b^2S^2)^{1/2}\cong 1/\sqrt{3}\ .$$

The desired convergence determines $S=M$, e.g., $|V(L_M)-V(L_{M-1})|<10^{-8}$ hartree before changing L to $L+1$ until the same convergence is reached between $V(L_M)$ and $V(L+1_M)$. Integration of $V^{(2)}$ from $H=K=M$ to ∞ and $L=L_M$ to ∞ yields

$$|V_{\text{correction}}|\simeq\left|\sum_M MV_{MML}\right|+|L_M(V(L_M)-V(L-1_M))|$$

$$\leq 10^{-6}\text{ hartree}\ .$$

Computations were done using an IBM RS6000. Unlike earlier methods for computing E_{Madelung} the UNIX codes in real space can be modified to introduce defects at any unit cell in order to represent the real materials. Convergence is achieved for $L=\pm 1$ and $M\leq 500$ to $1/10^3$ in less than 1 s and to $1/10^{12}$ in less than 3 s for the NaCl fcc unit cell, verifying that the codes can reproduce the Ewald construction method rapidly. The contribution from the unit cell to the Madelung constant is 1.456 03 and the rest contribute 0.291 53 to obtain 1.747 56 for the first five layers $L=0,\pm 1,\pm 2$, indicating that the contributions to the potential energy at the origin unit cell from layers with $L\geq 2$ are negligible because the dominating term in the sum (A1), $V^{(2)}_{HKL}$, cancels out the distant-plane contributions by symmetry. It takes several hours for the more complex structures I and IV.

*Author to whom all correspondence should be sent. Electronic address: acrivos@sjsuvml.edu

†Present address: Mat. Res. Lab. Ind. Tech. Res. Inst. Hsinchu, Taiwan.

‡Present address: Morris Research Inc., Berkeley, CA 94704.

[1](a) Y. Hayashi, M. Fukui, T. Fujita, H. Shibayama, K. Iwahashi, and K. Adachi, Jpn. J. Appl. Phys. **28**, L910 (1989); (b) Y. Hayashi, S. Sako, M. Fukui, T. Fujita, H. Sasakura, S. Minamigawa, and K. Nakahigashi, *ibid.* **28**, L1531 (1989); (c) J. V. Acrivos, M. Chen Lei, C. Jiang, H. Nguyen, P. Metcalf, and G. M. Honig, J. Solid State Chem. **111**, 343 (1994).

[2](a) N. F. Mott, Supercond. Sci. Technol. **4**, S59 (1991); (b) M. Kaveh and N. F. Mott, Phys. Rev. Lett. **68**, 1904 (1992); (c) J. V. Acrivos and O. Stradella, Int. J. Quantum Chem. **46**, 55 (1993); (d) Z. Kakol, J. Spałek, and J. M. Honig, J. Solid State Chem. **79**, 288 (1989); A. S. Alexandrov and N. F. Mott, Phys. Rev. Lett. **71**, 1075 (1993).

[3](a) M. R. Beasley, in *Advances in Superconductivity,* edited by K. Kitazawa and T. Ishiguro (Springer-Verlag, New York, 1989), p. 3; (b) J. K. Burdett and T. Hughbanks, J. Am. Chem. Soc. **106**, 3101 (1984); (c) J. B. Goodenough, Prog. Solid State Chem. **5**, 145 (1971); (d) J. K. Hulm, C. K. Jones, R. Hein, and J. W. Gibson, J. Low Temp. Phys. **7**, 291 (1972); (e) J. W. Lynn, *High Temperature Superconductivity* (Springer-Verlag, New York, 1990), Chap. 8.

[4](a) J. Spałek, Z. Kakol, and J. M. Honig, Solid State Commun. **7**, 511 (1989); (b) K. S. Nanjundaswamy, A. Lewicki, Z. Kakol, P. Gopalan, P. Metcalf, J. M. Honig, C. N. R. Rao, and J. Spałek, Physica C **166**, 361 (1989); (c) H. A. Blackstead, D. B. Pulling, J. Spałek, and J. M. Honig, Solid State Commun. **80**, 405 (1991); (d) Y. Takeda, R. Kanno, M. Sakano, O. Yamamoto, M. Takano, Y. Bando, H. Akinaga, K. Takita, and J. B. Goodenough, Mater. Res. Bull. **25**, 293 (1990); (e) V. Bhat, C. N. R. Rao, and J. M. Honig, Solid State Commun. **81**, 751 (1992).

[5](a) J. Stankowski, P. K. Kahol, N. S. Dalal, and J. S. Moodera, Phys. Rev. B **36**, 7126 (1987); (b) A. M. Portis, K. W. Blazey, and F. Waldner, Physica C **153 – 155**, 308 (1989); (c) C. D. Jeffries, Q. H. Lam, Y. Kim, C. M. Kim, A. Zettl, and M. P. Klein, Phys. Rev. B **39**, 11 526 (1989); (d) J. V. Acrivos, R. Ithnin, C. Bustillo, M. Chen Lei, and D. Hellmoldt, Physica C **162 – 164**, 1665 (1990); (e) L. Kevan, J. Bear, M. Puri, Z. Panz, and C. L. Yao, Am. Chem. Soc. Symp. Ser. **58**, 1143 (1988); (f) R. Jones, R. Janes, R. Armstrong, K. K. Singh, P. P. Edwards, D. J. Keeble, and M. R. Harrison, J. Chem. Soc. Faraday Trans. **86**, 683 (1990); (g) Y. Maniwa, A. Grupp, F. Hentsch, and M. Mehring, Physica C **156**, 755 (1988); (h) F. G. Adrian and D. O. Cowan, Chem. Eng. News **70**, 40 (1992), and references therein; (i) J. B. Torrance and R. M. Metzger, Phys. Rev. Lett. **63**, 1515 (1989); (j) C. Kessler, B. Nebedahl, D. Peligrad, A. Dulçic, H. U. Habermeier, and M. Mehring, Physica C **219**, 233 (1994); (k) L. S. Gosh, L. F. Cohen, J. C. Gallop, and A. D. Caplin, Physica C (to be published); (l) H. A. Blackstead and J. D. Dow, Pis'ma Zh. Eksp. Teor. Fiz. **59**, 262 (1994) [JETP Lett. **59**, 283 (1994)].

[6](a) C. Kittel, *Introduction to Solid State Physics* (Wiley, New York, 1986), Chap. 12, Problem 6; (b) J. M. Rowell, Phys. Rev. Lett. **11**, 200 (1963); (c) M. Peshkin and A. Tonomura, *The Aharonov-Bohm Effect*, Lecture Notes in Physics Vol. 340 (Springer-Verlag, New York, 1989), p. 192; (d) K. Harada, T. Matsuda, J. Bonevich, M. Igarashi, S. Kondo, G. Pozzi, U. Kawabe, and A. Tonomura, Nature **360**, 51 (1992) and Phys. Rev. Lett. **71**, 3371 (1993); (e) E. J. Pakidis and C. Jeffries, Phys. Rev. Lett. **47**, 1959 (1981); (f) C. Jeffries (private communication); (g) J. Ubbink, J. A. Poulis, H. J. Gerristen, and C. J. Gorter, Physica **18**, 361 (1952).

[7]J. M. Honig, G. Yuochunas, T. B. Reed, and E. R. Pollard, J. Cryst. Growth **30**, 42 (1975).

[8](a) J. W. Loram, K. A. Mirza, and R. S. Liu, Supercond. Sci. Technol. **4**, S286 (1991); (b) T. Tsurumi, T. Iwata, Y. Tajima, and M. Hikita, Jpn. J. Appl. Phys. **27**, L1616 (1988); R. S. Liu, J. M. Liang, S. F. Wu, Y. T. Huang, P. T. Wu, and L. J. Chen, Physica C **159**, 385 (1989); (d) K. K. Singh, W. Morris, Lei Chen, H. Nguyen, and J. V. Acrivos (unpublished); (e) J. V. Acrivos, M. Chen Lei, C. Jiang, H. Nguyen, P. Metcalf, and G. M. Honig (unpublished).

[9](a) J. E. Wertz, F. O. Koelsch, and J. Vivo' (Acrivos), J. Chem. Phys. **23**, 2194 (1955); (b) J. V. (Vivo') Acrivos, P. Hughes, and S. S. P. Parkin, *ibid.* **86**, 1780 (1987).

[10]A. Abragam and B. Bleaney, *Electron Paramagnetic Resonance of Transition Ions* (Clarendon, Oxford, 1970).

[11](a) J. V. Acrivos, J. Chem. Phys. **36**, 1097 (1962); J. V. Acrivos and J. Azebu, J. Magn. Reson. **4**, 1 (1971); (b) J. V. Acrivos, J. Chem. Phys. **47**, 5389 (1967).

[12](a) W. A. Little (unpublished); (b) Y. Ando, H. Kubota, S. Tanaka, M. Aoyagi, H. Akoh, and S. Takada, Phys. Rev. B **47**, 5481 (1993); (c) Wenbin Yu, K. H. Lee, and D. Stroud, Phys. Rev. B **47**, 5906 (1993).

[13]E. Madelung, Phys. Z. **19**, 524 (1918).

[14]P. P. Ewald, Ann. Phys. (Leipzig) **54**, 519 (1917); **64**, 253 (1921).

[15]M. Born and H. Kun, *Dynamical Theory of Crystal Lattices* (Oxford University, London, 1985).